

Direct observation of Rogue Waves in optical turbulence using Time Microscopy

Pierre Suret,* Rebecca El Koussaifi, Alexey Tikan, Clément

Evain, Stéphane Randoux, Christophe Szwaj, and Serge Bielawski

Laboratoire de Physique des Lasers, Atomes et Molécules, UMR-CNRS 8523, Université de Lille, France

Centre d'Etudes et de Recherches Lasers et Applications (CERLA), 59655 Villeneuve d'Ascq, France

The formation of coherent structures in noise driven phenomena and in Turbulence is a complex and fundamental question [1]. A particularly important structure is the so-called Rogue Wave (RW) that arises as the sudden appearance of a localized and giant peak [2–4]. First studied in Oceanography, RWs have been extensively investigated in Optics since 2007 [5], in particular in optical fibers experiments on supercontinua [5–7] and optical turbulence [4, 8]. However the typical timescales underlying the random dynamics in those experiments prevented –up to now– the direct observation of isolated RWs. Here we report on the direct observation of RWs, using an ultrafast acquisition system equivalent to microscope in the time domain [9–12]. The RWs are generated by nonlinear propagation of random waves inside an optical fiber, and recorded with ~ 250 fs resolution. Our experiments demonstrate the central role played by “breathers-like” solutions of the one-dimensional nonlinear Schrödinger equation (1D-NLSE) in the formation of RWs [13].

Common oceans waves are weakly nonlinear random objects having nearly Gaussian statistics, while at the same time, RWs are waves of extremely large amplitude that occur more frequently than expected from the normal law [2–4]. The mechanisms underlying the generation of coherent structures such as RWs from the nonlinear propagation of random waves i.e., in turbulent flows, is a subject of very active debates and still represents an open question [8, 14–16].

From the theoretical point of view, the so-called *focusing* 1D-NLSE (see Eq. 1), which is a generic equation having an ubiquitous importance in Physics, plays a central role in this debate [2, 4, 17, 18]. In particular, the 1D-NLSE describes at leading order the physics of deep-water wave trains and nonlinear propagation in optical fibers [19]. The breather-like solutions of the 1D-NLSE, also called solitons on finite background, are now considered as being prototypes of RWs [13, 17, 20–22].

Despite the numerous experimental works devoted to optical RWs, [4–8, 18, 23] the direct observation of these coherent structures in the time domain has never been reported in the context of the nonlinear propagation of *random waves*. Randomness of the initial condition is

known to play a crucial role in the generation of RWs as it has been pointed out in the supercontinuum driven by noise [5–7, 18] or in optical turbulence [4, 8, 18, 24]

Contrary to the experiments performed in the spatial domain [25, 26], the fast time scales of fluctuations (picoseconds or less) involved in single-mode fiber experiments makes single-shot recording of RWs a particularly challenging task. Pioneer works hence naturally provided *indirect evidences* of RWs, using e.g. spectral filtering [5–7] or statistical measurement from optical sampling techniques [8].

In this Letter, we present direct single-shot recordings of optical RWs by using a specially-designed *Time Microscope* (TM) ultrafast acquisition system [9, 10, 12]. The temporal resolution of ~ 250 fs of our TM (see Methods and supplementary material) allows us to investigate the fast dynamics arising from the nonlinear propagation of random waves in an optical fiber (upper part of Fig. 1). Observations performed with the TM at the output of the fiber immediately reveals the emergence of intense peaks, with powers frequently exceeding the average power $\langle P \rangle$ by factors of 10-50 [see Fig 1(b-d) and supplementary movie 1]. Starting from random fluctuations having typical time scale around 5 – 10ps [Fig 1(a)], those extreme peaks are also found to be extremely narrow, with time scales of the order of several hundreds of femtoseconds [Fig 1(b-d) and Fig 3(b-d)].

More precisely, the random waves used as initial conditions in our experiments are partially coherent light waves emitted by a high power Amplified Spontaneous Emission (ASE) light source at a wavelength $\lambda \sim 1560$ nm (see Fig. 1). Using a programmable optical filter, the optical spectrum of the partially coherent light is precisely designed to assume a Gaussian shape having a full width at half maximum that is adjusted either to $\Delta\nu = 0.1\text{THz}$ or $\Delta\nu = 0.05\text{THz}$. The partially coherent waves are launched into a 500 m-long single mode polarization maintaining fiber at a wavelength falling into the anomalous (focusing) regime of dispersion. The light at the output of the nonlinear fiber is then directed to the TM (detailed in Figure 2), which acquires traces (optical power versus time over a ≈ 20 ps-long window) at a rate of 500 per second, and displays the signals in real time.

As in a standard spatial imaging microscope, the TM is composed of an objective and a tube lens [see Fig. 2.(b)]. The objective is a time lens [9, 10, 12] operating from sum-frequency generation (SFG) between the 1560 nm

* Corresponding author : Pierre.Suret@univ-lille1.fr

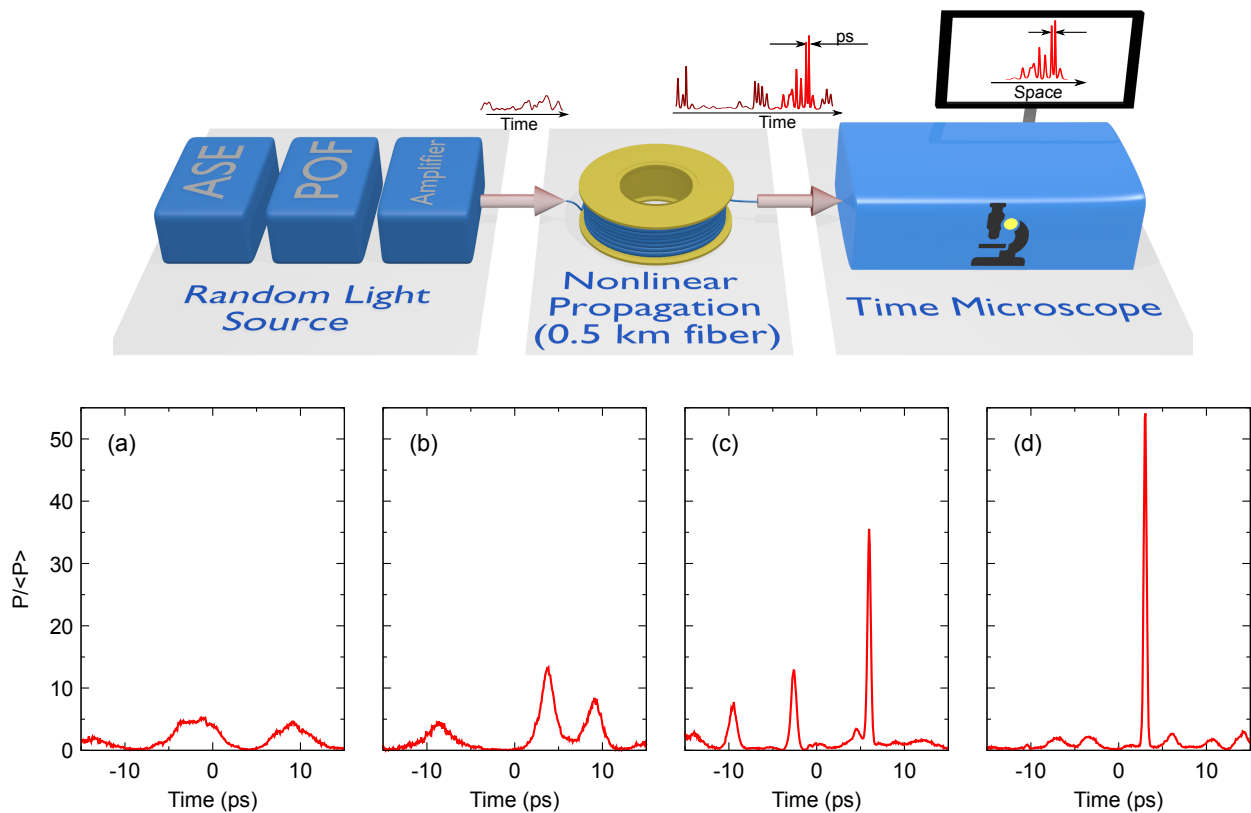


Figure 1. **Overview of Experiments** (Upper part) Global strategy for the experimental observation of optical rogue waves. Incoherent light from an 1560 nm Amplified Spontaneous Emission source (ASE) is filtered by using a Programmable Optical Filter (POF) and amplified before experiencing nonlinear propagation in a polarization maintaining (PM) fiber. Random fluctuations of the output power are analyzed in single-shot with sub-picosecond resolution, using a specially designed time-microscope, which maps the temporal evolution onto the spatial coordinate of a conventional camera (see Fig 2 and Methods for details). (a-d) Typical single-shot recordings of random waves. Initial spectral width $\Delta\nu = 0.1\text{THz}$. (a) Initial condition. (b-d) RWs observed at the output of the fiber for mean powers $\langle P \rangle = 0.5\text{W}$ (b), $\langle P \rangle = 2.6\text{W}$ (c), $\langle P \rangle = 4\text{W}$ (d)

signal and a chirped pump pulse (at 800 nm) (see Sec. Methods). The observation in the focal plane of the tube lens is achieved by a spectrum analyser (composed of a diffraction grating, a lens and a camera). The use of this TM strategy enables to easily reach extremely high dynamical ranges (up to 40 dB, see Methods), which is a crucial point for analyzing extreme events embedded in moderate power fluctuations.

In order to quantify the emergence of RWs, we compute statistical distributions from a large amount of data recorded with the TM at the input and at the output ends of the fiber (see Sec. Methods). As expected, the probability density function (PDF) of the optical power emitted by the ASE source is systematically very close to the exponential distribution that correspond to a Gaussian statistics for the field [see Fig. 3.(a)] [8, 15, 27]. On the contrary, the PDF of light power at the output of the nonlinear fiber is found to exhibit heavy-tailed deviations from the exponential distribution, thus confirming the generation of RWs [see Fig. 3.(a)]. Moreover the PDFs demonstrate that the number of RWs having high peak power increases while the mean power $\langle P \rangle$ of random op-

tical waves (*i.e.* the strength of nonlinearity) increases [see Fig. 3.(a)].

To the best of our knowledge, experimental signals plotted in Figs. 1.(a-d) and 3.(b-h) represent the first direct and accurate observation of the RWs underlying these heavy tailed statistics. Starting from random light propagating with a mean power of 4 W in the fiber, huge RWs having peak power that exceeds 300 W can be observed at the output of the fiber [Fig.3.(d)]. From a careful analysis of the data, two typical shapes can be distinguished : isolated breather-like RWs [see Fig. 3.(b)] and more complicated structures composed of several peaks [see Fig. 3.(c)]. In order to illustrate the process of emergence of breather like RWs, we plot in Fig. 3.(e-h) different structures observed after the propagation of partially coherent waves having an initial spectral width $\Delta\nu = 0.05\text{THz}$ and an average power $\langle P \rangle = 0.3\text{W}$. We have selected these structures because their shapes are strikingly similar to those found in the scenario leading to the formation of the Peregrine soliton (PS) while starting from a single hump at initial stage [28]. Remarkably, the *power profile* of the exact

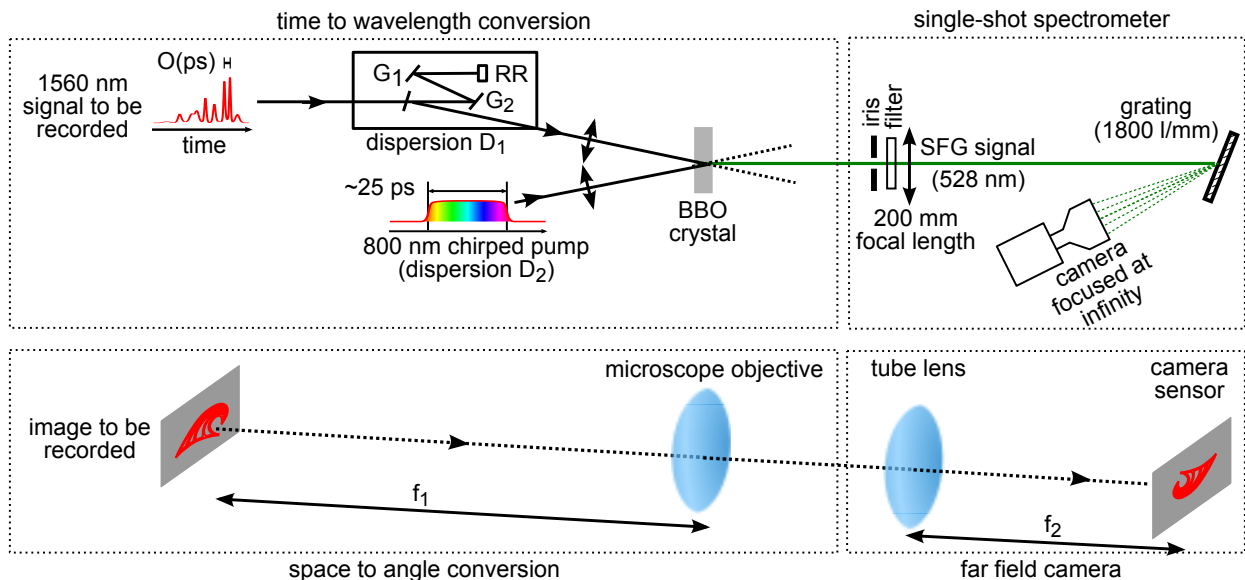


Figure 2. **Time microscope realized for the ultrafast acquisition of rogue waves.** Upper part: experimental setup. A key element is the time lens, which is composed by the BBO crystal, pumped by the stretched 800 nm pulse. Lower part: spatial analog of the time microscope. The dispersion D_1 (provided by the grating compressor) is analog to the diffraction between the initial image and the lens with focal length f_1 . The time lens is the analog of the (f_1) lens. The single-shot spectrometer is formally analog to the far-field camera. G_1 and G_2 are 600 l/mm gratings, RR is a roof retroreflector. Note that the BBO crystal is placed at the focal plane of the 200 mm collimating lens. Transport optics are not represented.

analytical PS coincide very well with experimental structures [see green dashed line in 3.(h)]. However note that the precise identification of the breathers-like structures (as PS or Akhmediev breather or other more complex solutions of 1D-NLSE) would require a simultaneous measurement of the phase dynamics [29].

Behaviors observed in experiments can be well reproduced from numerical simulations of the 1D-NLSE (see Sec. Methods). First of all, the PDFs of optical power [see Fig. 4.(a)] and the optical spectra (see Supplementary Material) are well reproduced by numerical simulations. Fig. 4 shows a picture of typical random fluctuations of the optical power that are found at the input and output ends of the optical fiber. Taking a partially-coherent light field having a bandwidth of 0.1 THz at initial stage, the typical time scale for power fluctuations is around a few picoseconds [Fig. 4(b)]. The scenario observed in the experiments are also found in numerical simulations. In particular, either breather-like structures appear and disappear along the propagation [see Fig.4(g)], either several pulses simultaneously emerge together from the random background [see Fig. 4(c)]. Our experiments provide snapshots randomly recorded while the numerical simulations allow to follow the dynamics of nonlinear random waves along the propagation. In this respect, the numerical simulations

reveal that the breather-like structures often emerge on the top of the initial power fluctuations (see Fig. 4(d-g) and video in Supplementary Material).

In the last years, the common and shared conjecture is that breather-like solutions of 1D-NLSE such as PS or Akhmediev breathers represent prototypes of RWs [13, 16–18, 20–22]. This has motivated very nice experiments in which these solitons on finite background have been generated in a deterministic way in optical fibers [20, 22, 30] and in a one-dimensional water tank [21]. These experiments make use of carefully-designed *coherent initial conditions*.

On the contrary, the initial conditions in our experiments are designed to be “ocean-like” *random waves* [4, 31]. In this context of nonlinear propagation of random waves, previous experimental works performed in a 1D water tank [32] and in optical fibers [8] have revealed heavy-tailed deviations from Gaussian statistics. For the first time, our time-resolved observations correlate in an unambiguous way the occurrence of this heavy-tailed statistics with the frequent occurrence of breather-like coherent structures. Our experimental observations favor a well-known scenario in which a PS emerges from a single real hump [28]. However it must be emphasized that the precise identification of coherent structures requires the precise knowledge of the phase

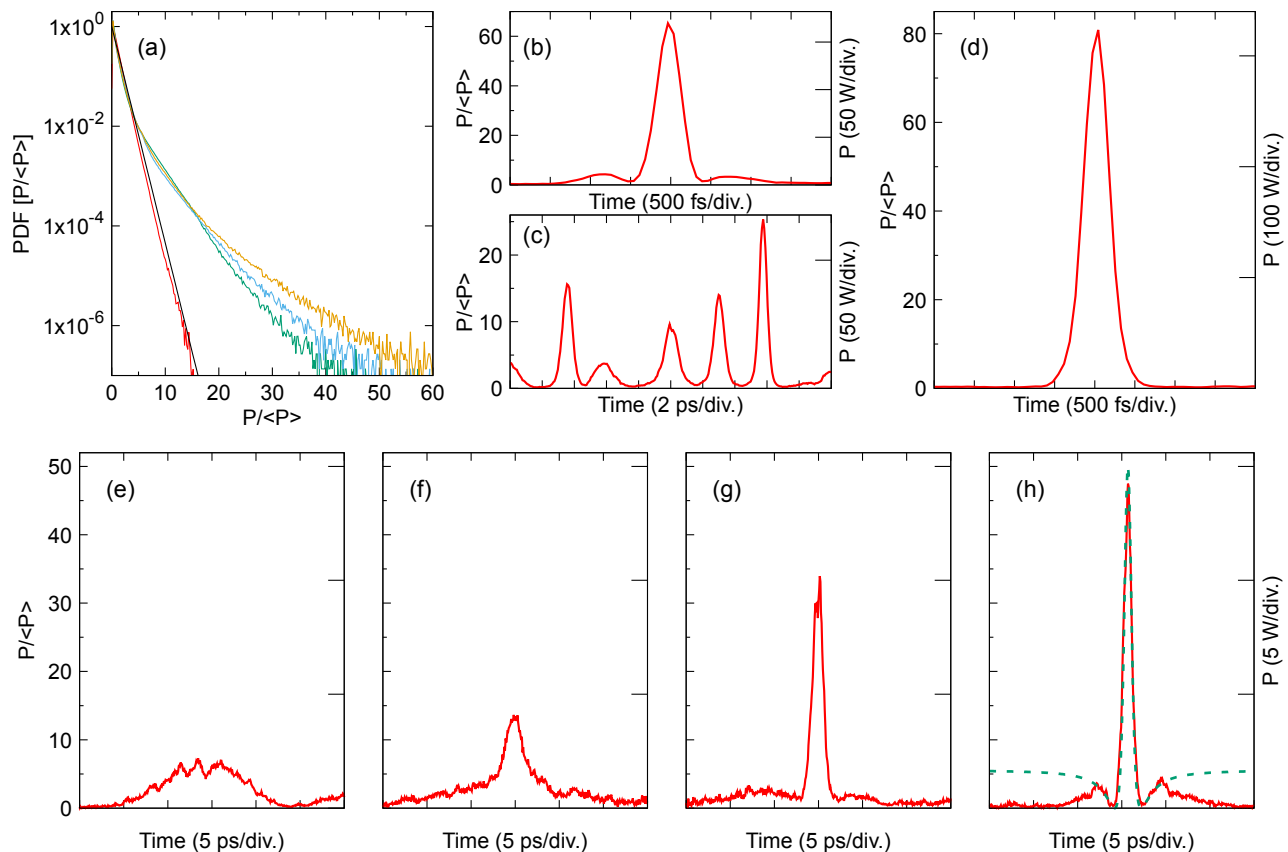


Figure 3. **Typical power profiles and Statistics of Rogue Waves (Experiments)** (a) PDF of the initial condition (red line) and of the output power at 500 mW (green line), 2.6 W (blue line), 4 W (yellow line). The black line represents the normalized exponential distribution : $\text{PDF}(P/\langle P \rangle) = \exp(-P/\langle P \rangle)$. (b-d) Typical random signals recorded by the TM at the output of the nonlinear PM fiber. (b) PS-like structure ($P = 2.6$ W, $\Delta\nu = 0.1$ THz). (c) Series of multiple peaks ($P = 2.6$ W, $\Delta\nu = 0.1$ THz). (d) Giant optical RW reaching a peak power ~ 80 times greater than the mean power of the random wave ($P = 4$ W, $\Delta\nu = 0.1$ THz). (e-h) Typical snapshots showing several stages leading to the emergence of a breather-like structure ($P = 300$ mW, $\Delta\nu = 0.05$ THz). The green dashed line in (h) represents the best fit to the analytical expression of a PS.

evolution. The simultaneous fast measurement of phase and amplitude fluctuations therefore represents the next experimental bottleneck for the careful identification of optical RWs.

The emergence of coherent structures is a general and mysterious feature of stochastically driven processes such as turbulence, supercontinuum generation or pattern formation [1, 18, 33]. The time-resolved direct observation of RWs presented in the letter opens the way to numerous studies on the relationship between coherent structures and noise driven phenomena. In particular, shot by shot *spectral* measurements in pulsed experiments recently revealed the fascinating complexity of the statistical features associated to the so called modulation instability [33]. By using our TM, the underlying dynamics of the so-called process of noise-driven modulational instability and its nonlinear stage is an open fundamental question that can now be studied [15, 33].

METHODS

The partially coherent light (i.e., the initial condition) is generated by an Erbium fiber broadband Amplified Spontaneous Emission (ASE) source (Highwave), which is spectrally filtered (with programmable shape and linewidth) using a programmable optical filter (Waveshaper 1000S, Finisar). The output is then amplified by an Erbium-doped fiber amplifier (Keopsys). This random light is launched into a single-mode polarization maintaining fiber (Fibercore HB-1550T), with 500 m length and a dispersion $\beta_2 = -20$ ps²km⁻¹ (measured). For a given spectral width, the power of the light launched inside the fiber is controlled using a half wavelength plate and a polarizing cube.

For the single-shot acquisition of the sub-picosecond optical signals, we realized an *upconversion time-microscope*, largely based on the work of Ref. [10]. From the input-output point of view, the time microscope encodes the temporal shape of the optical signal onto the

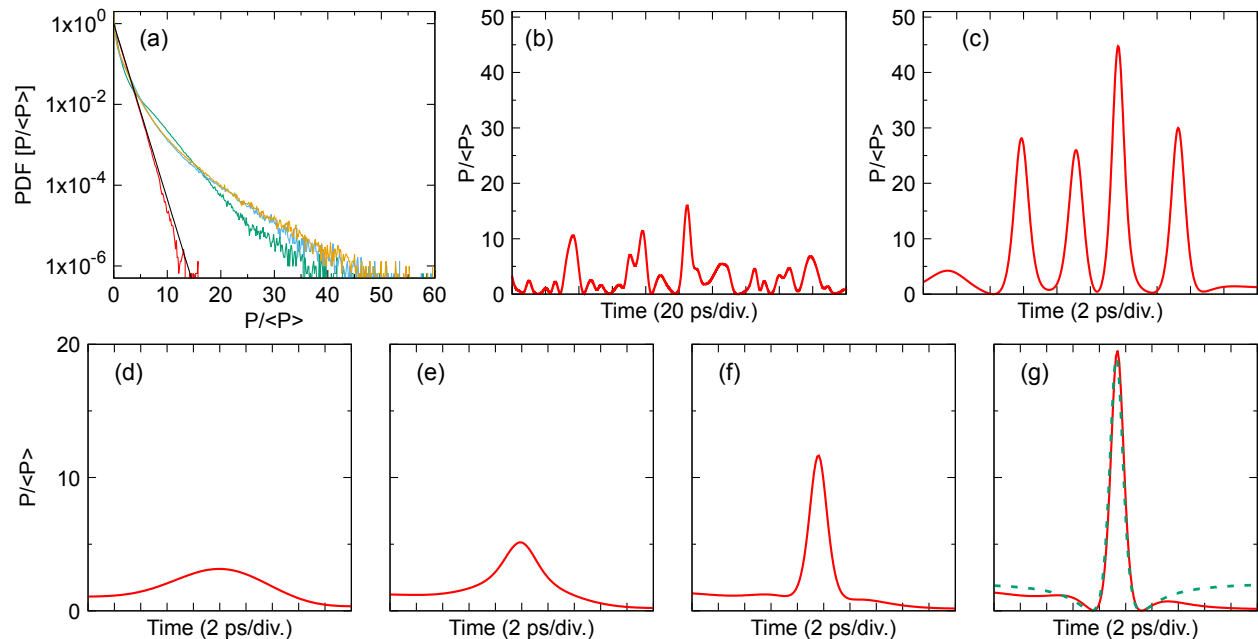


Figure 4. **Typical power profiles and Statistics of Rogue Waves (Numerical Simulations of the 1D-NLSE)** (a) PDF of the initial condition (red line) and of the output power at 500 mW (green line), 2.6 W (yellow line), 4 W (blue line). The black line represents the normalized exponential distribution : $\text{PDF}(P/\langle P \rangle) = \exp(-P/\langle P \rangle)$. (b) Typical fluctuations of the power of the random field used as initial condition. (c) Series of multiple peaks (zoom) ($P = 2.6$ W, $\Delta\nu = 0.1$ THz). (d-h) Typical snapshots (zoom) showing several stages leading to the emergence of a breather-like structure along the propagation ($P = 1$ W, $\Delta\nu = 0.05$ THz, $z = 0$ (d), $z = 285$ (e), $z = 415$ m, (f) $z = 500$ m). The green dashed line in (g) represents the best fit to the analytical expression of a PS.

spectrum of a chirped pulse (i.e., spectral encoding). Then the spectrum is recorded using a simple spectrometer composed of a 1800 l/mm grating and a sCMOS camera. A region of interest (of typically 2048x8 pixels) is selected for recording the image (a raw image is presented in Fig. 2 of the supplementary material).

For reaching high temporal resolution, a key element is the time-lens [9], which is composed by a BBO crystal, pumped by a chirped 800 nm pulse. Before entering the time lens, the 1560 nm signal experiences anomalous dispersion in a classic Treacy grating compressor (see Fig. 2).

As in other time-lens systems [9–12] high resolution requires proper adjustment of the 1560 nm compressor (see supplemental material for adjustment detail, and performances of the setup). Conceptually, this is exactly analog to the tuning of the object-microscope objective distance in classical microscopes. For all results presented in this paper, the temporal resolution is 250 fs FWHM, and the field of view is of the order of 20 ps.

As another crucial point, the time-microscope strategy leads to an extremely high dynamical range (i.e., the ratio between maximal recordable signal and dark noise). This directly stems from the choice of employing a camera for the recording. More precisely, our 16 bit sCCD camera has an RMS dark noise of ≈ 2 electrons and a saturation value of 30000 electrons, leading to a ≈ 40 dB dynamical range.

The 800 nm pump is provided by an amplified Titanium-Sapphire laser (Spectra Physics Spitfire, 2 mJ, 40 fs, a spectral bandwidth of about 25 nm), operated at 500 Hz, and only 20 nJ are typically used here. For inducing (normal) dispersion on the 800 nm pulses we simply adjusted the amplifier’s output compressor. The dispersion was fixed to 0.23 ps², leading to chirped pulses of duration of about 20 ps. The 1560 nm grating compressor uses two 600 l/mm gratings, operated at an angle of incidence of 40 degrees, and whose planes are separated by 42 mm. The BBO crystal has 8 mm length and is cut for noncollinear type-I SFG. Focusing of the 800 nm and 1560 nm signals on the BBO crystal are performed by two lenses with 20 cm focal lengths. In order to improve the rejection of the 800 nm and the 1560 nm and to keep only the SFG at 528 nm, a 40-nm bandpass filter around 531 nm (FF01 531/40-25 Semrock) is added after the crystal. The camera is a sCMOS Hamamatsu Orca flash 4.0 V2 (C11440-22U), equipped with a 80 mm lens (Nikkor Micro 60 mm f/2.8 AF-D). The objective is focused at infinity and the waist of the SFG in the BBO crystal is imaged on the camera sensor. The camera is synchronized on the 800 nm laser pulses, and the integration time is adjusted to 1 ms, thus enabling single-shot operation of the time-microscope. PDFs of optical power are computed with $75 \cdot 10^6$ samples (10^2 points taken in the center of the temporal field of the TM from $75 \cdot 10^4$ frames) for a given set of parameters.

Numerical simulations are performed by integrating the 1D-NLSE :

$$i \frac{\partial \psi}{\partial z} = \frac{\beta_2}{2} \frac{\partial^2 \psi}{\partial t^2} - \gamma |\psi|^2 \psi, \quad (1)$$

where ψ is complex envelope of the electric field, normalized so that $|\psi|^2$ is the optical power, z is the longitudinal coordinate in the fiber, and t is the retarded time. $\beta_2 = -20 \text{ ps}^2 \text{ km}^{-1}$ is the second-order dispersion coefficient of the fiber and $\gamma = 2 \text{ W}^{-1} \text{ km}^{-1}$ is the Kerr coupling coefficient. All numerical integrations are performed using an adaptive stepsize pseudospectral method, using a mesh of 2048 points, over a temporal window of $\Delta T = 250 \text{ ps}$.

In numerical simulations presented in this letter, we neglect linear losses ($\simeq 0.5 \text{ dB}$) and stimulated Raman scattering. These approximations provide quantitative agreement between experiments and numerical simulations at moderate powers ($< 2 \text{ W}$). Additional numerical simulations show that stimulated Raman scattering has to be taken into account in order to reproduce very precisely the experimental PDFs and optical spectra at high values of the mean power (*i.e.* $\langle P \rangle = 4 \text{ W}$). However the main physical results (formation of RWs, emergence of breather-like structures and heavy-tailed PDFs) are not affected by stimulated Raman scattering.

The random complex field $\psi(t, z = 0)$ used as initial condition in numerical simulations is made from a dis-

crete sum of Fourier components :

$$\psi(z = 0, t) = \sum_m \widehat{X}_m e^{im\Delta\omega t}. \quad (2)$$

with $\widehat{X}_m = \frac{1}{\Delta T} \int_0^{\Delta T} \psi(z = 0, t) e^{-im\Delta\omega t} dt$ and $\Delta\omega = 2\pi/\Delta T$. The Fourier modes $\widehat{X}_m = |\widehat{X}_m| e^{i\phi_m}$ are complex variables. We have used the so-called random phase (RP) model in which only the phases ϕ_m of the Fourier modes are considered as being random [34]. In this model, the phase of each Fourier mode is randomly and uniformly distributed between $-\pi$ and π . Moreover, the phases of separate Fourier modes are not correlated so that $\langle e^{i\phi_n} e^{i\phi_m} \rangle = \delta_{nm}$ where δ_{nm} is the Kronecker symbol ($\delta_{nm} = 0$ if $n \neq m$ and $\delta_{nm} = 1$ if $n = m$). With the assumptions of the RP model above described, the statistics of the initial field is stationary, which means that all statistical moments of the complex field $\psi(z = 0, t)$ do not depend on x [24]. In the RP model, the power spectrum $n_0(\omega)$ of the random field $\psi(z = 0, t)$ reads as :

$$\langle \widehat{X}_n \widehat{X}_m \rangle = n_{0n} \delta_{nm} = n_0(\omega_n). \quad (3)$$

with $\omega_n = n \Delta\omega$. In our simulations, we have taken a random complex field $\psi(z = 0, t)$ having a Gaussian optical power spectrum that reads

$$n_0(\omega) = n_0 \exp \left[- \left(\frac{\omega^2}{\Delta\omega^2} \right) \right] \quad (4)$$

where $\Delta\omega = 2\pi\Delta\nu$ is the half width at $1/e$ of the power spectrum. Statistical properties of the random wave have been computed from Monte Carlo simulation made with an ensemble of 10^5 realizations of the random initial condition.

-
- [1] Sirovich, L. Turbulence and the dynamics of coherent structures. part i: Coherent structures. *Quarterly of applied mathematics* **45**, 561–571 (1987).
- [2] Onorato, M., Osborne, A. R., Serio, M. & Bertone, S. Freak waves in random oceanic sea states. *Phys. Rev. Lett.* **86**, 5831–5834 (2001).
- [3] Kharif, C., Pelinovsky, E. & Slunyaev, A. *Rogue Waves in the Ocean* (Springer, Heidelberg, 2009).
- [4] Onorato, M., Residori, S., Bortolozzo, U., Montina, A. & Arecchi, F. Rogue waves and their generating mechanisms in different physical contexts. *Physics Reports* **528**, 47 – 89 (2013).
- [5] Solli, D. R., Ropers, C., Koonath, P. & Jalali, B. Optical rogue waves. *Nature* **450**, 1054–1057 (2007).
- [6] Erkintalo, M., Genty, G. & Dudley, J. M. Rogue-wave-like characteristics in femtosecond supercontinuum generation. *Opt. Lett.* **34**, 2468–2470 (2009).
- [7] Mussot, A. *et al.* Observation of extreme temporal events in cw-pumped supercontinuum. *Opt. Express* **17**, 17010–17015 (2009).
- [8] Walczak, P., Randoux, S. & Suret, P. Optical rogue waves in integrable turbulence. *Phys. Rev. Lett.* **114**, 143903 (2015). URL <http://link.aps.org/doi/10.1103/PhysRevLett.114.143903>.
- [9] Kolner, B. H. & Nazarathy, M. Temporal imaging with a time lens. *Optics letters* **14**, 630–632 (1989).
- [10] Bennett, C. & Kolner, B. Upconversion time microscope demonstrating 103× magnification of femtosecond waveforms. *Optics letters* **24**, 783–785 (1999).
- [11] Foster, M. A. *et al.* Silicon-chip-based ultrafast optical oscilloscope. *Nature* **456**, 81–84 (2008).
- [12] Okawachi, Y. *et al.* Asynchronous single-shot characterization of high-repetition-rate ultrafast waveforms using a time-lens-based temporal magnifier. *Opt. Lett.* **37**, 4892–4894 (2012). URL <http://ol.osa.org/abstract.cfm?URI=ol-37-23-4892>.
- [13] Akhmediev, N., Ankiewicz, A. & Taki, M. Waves that appear from nowhere and disappear without a trace. *Physics Letters A* **373**, 675 – 678 (2009).
- [14] Hammani, K., Kibler, B., Finot, C. & Picozzi, A. Emergence of rogue waves from optical turbulence. *Physics Letters A* **374**, 3585 – 3589 (2010).

- [15] Agafontsev, D. S. & Zakharov, V. E. Integrable turbulence and formation of rogue waves. *Nonlinearity* **28**, 2791 (2015). URL <http://stacks.iop.org/0951-7715/28/i=8/a=2791>.
- [16] Toenger, S. *et al.* Emergent rogue wave structures and statistics in spontaneous modulation instability. *Scientific Reports* **5** (2015).
- [17] Akhmediev, N., Dudley, J. M., Solli, D. R. & Turitsyn, S. K. Recent progress in investigating optical rogue waves. *Journal of Optics* **15**, 060201 (2013).
- [18] Dudley, J. M., Dias, F., Erkintalo, M. & Genty, G. Instabilities, breathers and rogue waves in optics. *Nat. Photon.* **8**, 755 (2014).
- [19] Chabchoub, A. *et al.* The nonlinear schrödinger equation and the propagation of weakly nonlinear waves in optical fibers and on the water surface. *Annals of Physics* **361**, 490 – 500 (2015). URL <http://www.sciencedirect.com/science/article/pii/S0003491615002687>.
- [20] Kibler, B. *et al.* The peregrine soliton in nonlinear fibre optics. *Nature Physics* **6**, 790–795 (2010).
- [21] Chabchoub, A., Hoffmann, N. P. & Akhmediev, N. Rogue wave observation in a water wave tank. *Phys. Rev. Lett.* **106**, 204502 (2011).
- [22] Kibler, B. *et al.* Observation of kuznetsov-ma soliton dynamics in optical fibre. *Scientific Reports* **2** (2012).
- [23] Hammani, K., Finot, C., Dudley, J. M. & Millot, G. Optical rogue-wave-like extreme value fluctuations in fiber raman amplifiers. *Opt. Express* **16**, 16467–16474 (2008).
- [24] Picozzi, A. *et al.* Optical wave turbulence: Towards a unified nonequilibrium thermodynamic formulation of statistical nonlinear optics. *Physics Reports* **542**, 1 – 132 (2014).
- [25] Bromberg, Y., Lahini, U., Small, E. & Silberberg, Y. Hanbury brown and twiss interferometry with interacting photons. *Nat. Photon.* **4**, 721–726 (2010).
- [26] Pierangeli, D., Di Mei, F., Conti, C., Agrat, A. J. & DelRe, E. Spatial rogue waves in photorefractive ferroelectrics. *Phys. Rev. Lett.* **115**, 093901 (2015). URL <http://link.aps.org/doi/10.1103/PhysRevLett.115.093901>.
- [27] Goodman, J. W. *Statistical optics* (1985).
- [28] Bertola, M. & Tovbis, A. Universality for the focusing nonlinear schrödinger equation at the gradient catastrophe point: Rational breathers and poles of the tritronquée solution to painlevé i. *Communications on Pure and Applied Mathematics* **66**, 678–752 (2013). URL <http://dx.doi.org/10.1002/cpa.21445>.
- [29] Randoux, S., Suret, P. & El, G. Identification of rogue waves from scattering transform analysis of periodized waveforms. *arXiv:1512.04707* (2015).
- [30] Frisquet, B., Kibler, B. & Millot, G. Collision of akhmediev breathers in nonlinear fiber optics. *Physical Review X* **3**, 041032 (2013).
- [31] Janssen, P. A. E. M. Nonlinear four-wave interactions and freak waves. *J. Phys. Oceanogr.* **33**, 863 (2003).
- [32] Onorato, M. *et al.* Observation of strongly non-gaussian statistics for random sea surface gravity waves in wave flume experiments. *Phys. Rev. E* **70**, 067302 (2004).
- [33] Solli, D., Herink, G., Jalali, B. & Ropers, C. Fluctuations and correlations in modulation instability. *Nature Photonics* **6**, 463–468 (2012).
- [34] Nazarenko, S. *Wave Turbulence*. Lecture Notes in Physics (Springer, 2011).

ACKNOWLEDGMENTS

This work was supported by the Labex CEMPI (ANR-11-LABX-0007-01) and by the French National Research Agency (ANR-12-BS04-0011 OPTIROC) and the BQR Émergence-Innovation of Lille 1 University. The authors are grateful to Francois Anquez and the Biophysics of Cellular Stress Response group of the PhLAM for the fruitful discussions, their crucial help, and for providing the sCMOS Camera. The authors are also grateful to Arnaud Mussot, Rémi Habert and the photonics group of the PhLAM for fruitful discussions, for the equipments (the ps laser), and for the measurement of the GVD of the fiber. The authors thank Nunzia Savoia for the everyday work on the femto laser and Marc Le Parquier for his crucial contribution in the development of the time-lens.